Continental Shelf Research 279 (2024) 105278

Contents lists available at ScienceDirect

Continental Shelf Research

journal homepage: www.elsevier.com/locate/csr

Continental shelf wave generation due to surface stress anomalies in the wake of offshore wind farms

Jan Erik H. Weber [a,*], Göran Broström [b]

[a] Department of Geosciences, University of Oslo, Norway
[b] Department of Marine Sciences, University of Gothenburg, Sweden

ARTICLE INFO

Keywords:
Continental shelf waves
Wind farms
Wind wakes
Resonance due to wind forcing

ABSTRACT

For isolated oceanic structures above sea level in synoptic-scale wind fields, shielding causes a wind wake with reduced wind intensity on the lee side of the structure. This generates a wind-stress curl that may act as a source term for continental shelf waves (CSWs) propagating around the structure, if the bottom is sloping. We investigate CSW propagation in the case where the structure (a wind farm or an island) is circular and the depth over the shelf slope increases exponentially with radial distance. For free waves, the wave number, and hence the frequency, is quantized. We demonstrate that for circular banks with narrow continental margins, the resulting eigenfrequencies are close to those obtained for a straight shelf. Modelling the stress in the wind wake as a solitary pulse that moves along a straight shelf, we find, in the absence of friction, a forced solution that increases linearly in time when the pulse moves with the same speed as the free wave speed. For strong winds over longer periods of time, the along-shore wave velocity in the case of resonance may be of the order m/s for topographic parameters characteristic of the Taiwan Bank. Velocities of this magnitude could potentially cause harmful erosion as well as affect the ecosystem on the bank slopes.

1. Introduction

Free CSWs are basically governed by the conservation of potential vorticity. The angular frequency is smaller than the inertial frequency, and the wave phase propagates with shallow water on the right-hand side in the northern hemisphere (Longuet-Higgins, 1965). For the case of a straight shelf, the classic treatment of free CSWs is that of Buchwald and Adams (1968); see e.g., the review by Brink (1991). For trapping around banks or islands, the results are qualitatively as for a straight shelf, except that the wavelength around the bank (and hence the frequency) is quantized (Huthnance, 2001).

Usually, CSWs are generated by the presence of synoptic-scale atmospheric low-pressure systems (typical dimensions 1000 km, or more) through the action of the surface wind-stress curl; see Gill and Schumann (1974) (hereafter referred to as GS74). This forcing may conveniently be divided into two parts; one which is a wind-stress curl that does not depend on depth, and one which is proportional to the cross-shore depth gradient times the alongshore wind stress. The latter is proportional to the Ekman transport towards the coast in the surface layer. For that reason, we denote this part as the Ekman forcing. The typical wavelength of a CSW is often very large (of the order of the synoptic storm scale). In that case, the associated depth-independent wind-stress curl is small and can be neglected in the wave generation process. Hence, the onshore-offshore Ekman forcing dominates in this case (GS74). Since the total normal flux must vanish at the shore, the resulting compensating offshore-onshore flow across isobaths at lower depths induces the vortex stretching associated with CSW propagation.

For offshore wind farms, the forcing conditions may be different. As shown in the reduced-gravity model study of wind farms by Broström (2008), a rather strong small-scale wind-stress curl (typical dimension 100 km) occurs in the wind wake; see also Christiansen et al. (2022). This forcing has a lateral extent of the same order as the width of the wind farm itself and creates upwelling and downwelling patterns through divergence in the upper-layer Ekman transport. However, for a wind farm with a sloping shelf, such a small-scale wind-stress curl may also induce CSWs with a wavelength that is comparable to the lateral dimension of the wind farm. Hence, it should be possible to have CSWs propagating along the bottom contours of wind farms. In this case, the depth-independent wind-stress curl may be of the same order, or larger, than the previously described Ekman forcing by GS74. We will demonstrate that this is the case for the forcing by a wind that changes direction, and hence induces a wake that moves around the bank.

* Corresponding author.
E-mail addresses: j.e.weber@geo.uio.no (J.E.H. Weber), goran.brostrom@marine.gu.se (G. Broström).

https://doi.org/10.1016/j.csr.2024.105278
Received 22 February 2024; Received in revised form 20 May 2024; Accepted 1 July 2024
Available online 2 July 2024

The environmental consequences of CSWs could be important. The wave velocity components may enhance the amount of bottom material in suspension, and the associated Lagrangian mean drift (Weber and Drivdal, 2012) may redistribute suspended sediments, organic material and pollution. The group velocity of the CSWs (and hence the energy flux) will depend on the shelf geometry, and may be positive, negative or even zero for realistic geometries. In the last case, there will be an accumulation of wave energy in the region (the wind wake) where the waves are generated. Furthermore, if the wind stress field move with the same speed as that of free CSWs, resonance may occur. This may lead to large current velocities (of the order m/s) which could cause harmful erosion and increased vertical mixing.

The rest of this paper is structured as follows: Section 2 presents the mathematical formulation of this problem and Section 3 describes the motion in cylindrical polar coordinates. Section 4 discusses free CSWs on a circular shelf and presents solutions in the form of Whittaker functions. In Section 5, we introduce an idealized bank geometry, and calculate eigenfrequencies for selected quantized wave numbers around the bank. Section 6 compares CSW solutions for a radially symmetric shelf and a straight shelf, and Section 7 solves the forced problem on a straight shelf for a wind-stress pulse moving with constant speed. In Section 8 we discuss the conditions for resonant forcing, and calculate the time-increasing wave velocity for strong winds. Finally, Section 9 contains a discussion and some concluding remarks.

2. Mathematical formulation

We consider CSWs in a barotropic ocean generated by wind stress at the surface. In Cartesian coordinates, the horizontal x, y axes are situated at the undisturbed ocean surface, and the z axis is directed vertically upwards. The ocean surface is given by $z = \eta(x, y, t)$, where t denotes time, and the bottom profile is $z = -H(x, y)$. Neglecting the effect of bottom friction, and using the shallow water approximation, we can write the linearized equations for the wave motion (GS74) as

$$U_t^{(x)} - fU^{(y)} = -gH\eta_x + T^{(x)}, \tag{1}$$

$$U_t^{(y)} + fU^{(x)} = -gH\eta_y + T^{(y)}, \tag{2}$$

$$\eta_t = -U_x^{(x)} - U_y^{(y)}. \tag{3}$$

Here f is the constant Coriolis parameter, g is the acceleration due to gravity, $U^{(x)}, U^{(y)}$ are the volume fluxes and $T^{(x)}, T^{(y)}$ are the surface wind stresses per unit density in the x and y directions, respectively. For brevity, we use subscripts to denote partial differentiation.

We assume that we can neglect the surface divergence η_t in (3), (but not the surface gradients in (1) and (2)). This is referred to as the rigid lid approximation. In that case, we can introduce a stream function ψ such that $U^{(x)} = -\psi_y$ and $U^{(y)} = \psi_x$. For this to be valid, the squared width B^2 of the shelf must be small compared to the squared barotropic Rossby radius of deformation gH_{mid}/f^2, i.e., $f^2B^2/(gH_{mid}) \ll 1$, where H_{mid} is an averaged depth over the shelf. A thorough discussion of the validity of this approximation is found in GS74 and Brink (1983).

2.1. A straight shelf

For didactic reasons, we first recapitulate this problem for a straight coast aligned along the x axis where $H = H(y)$, as in GS74; see Fig. 1.

Here $H = H_0 \exp(2by)$ for $0 \le y \le B$, where b is a measure of the steepness of the shelf slope. Furthermore, at the coast, $v(y = 0) = 0$. Cross-differentiating and adding (1) and (2), using the rigid lid approximation, we then obtain

$$\psi_{txx} + \psi_{tyy} - (H'/H)[\psi_{ty} + f\psi_x] = T_x^{(y)} - T_y^{(x)} + (H'/H)T^{(x)} \tag{4}$$

Here $' = d/dy$. For free waves over an exponential shelf, continued by a flat bottom (Buchwald and Adams, 1968), the boundary condition at the coast $y = 0$ is $\psi = 0$. At the shelf edge $y = B$, we must have continuity of volume fluxes and pressure (here surface elevation); see e.g., Weber and Drivdal (2012). This leads to

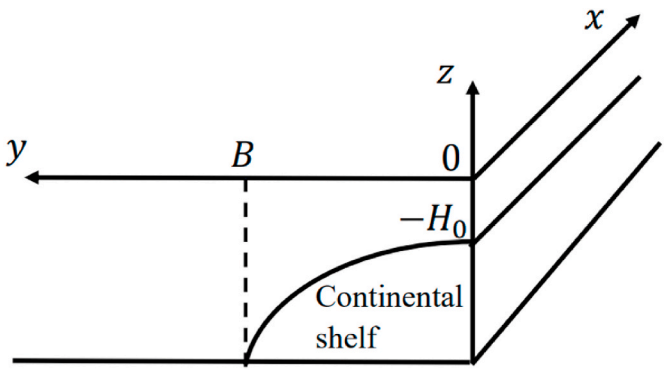

Fig. 1. Sketch of a straight continental shelf.

$$\psi_y + \kappa\psi = 0, \; y = B, \tag{5a}$$

where κ is the wave number in the x direction. In GS74, it was pointed out that for long CSWs, it is a good approximation to assume vanishing alongshore velocity at the slope edge, i.e.,

$$\psi_y(y = B) = 0. \tag{5b}$$

This also follows from (5a) for small wave numbers.

In GS74 the length scale in the x direction was assumed to be very large. Hence, the wind-stress curl $T_x^{(y)} - T_y^{(x)}$ on the right-hand side of (4) was assumed to be negligibly small compared to the Ekman forcing $(H'/H)T^{(x)}$. It is far from certain that these assumptions hold for a wind farm, so we must keep both forcing terms in (4). In the present paper, we consider isolated structures in the open ocean. To do that, it is convenient to introduce cylindrical polar coordinates.

3. Cylindrical geometry

We consider an idealized situation with a circular bank or island, and describe the motion in cylindrical polar coordinates r, θ, z. The radial and angular coordinates r, θ depend on the Cartesian coordinates x, y through the relations $x = r\cos\theta$, $y = r\sin\theta$. The angular coordinate θ, defined from the polar axis (here the x axis) is positive in the counter-clockwise direction; see Fig. 2.

Defining the radial and angular volume fluxes as

$$U^{(r)} = U^{(x)}\cos\theta + U^{(y)}\sin\theta, \tag{6}$$

$$U^{(\theta)} = -U^{(x)}\sin\theta + U^{(y)}\cos\theta, \tag{7}$$

equations (1) and (2) can be written

$$U_t^{(r)} - fU^{(\theta)} = -gH\eta_r + T^{(r)}, \tag{8}$$

$$U_t^{(\theta)} + fU^{(r)} = -gHr^{-1}\eta_\theta + T^{(\theta)}, \tag{9}$$

where the radial and angular wind stress components are

$$T^{(r)} = T^{(x)}\cos\theta + T^{(y)}\sin\theta, \tag{10}$$

$$T^{(\theta)} = -T^{(x)}\sin\theta + T^{(y)}\cos\theta. \tag{11}$$

Assuming rigid lid as before, the radial and angular volume fluxes become in terms of the stream function ψ:

$$U^{(r)} = -r^{-1}\psi_\theta, \tag{12}$$

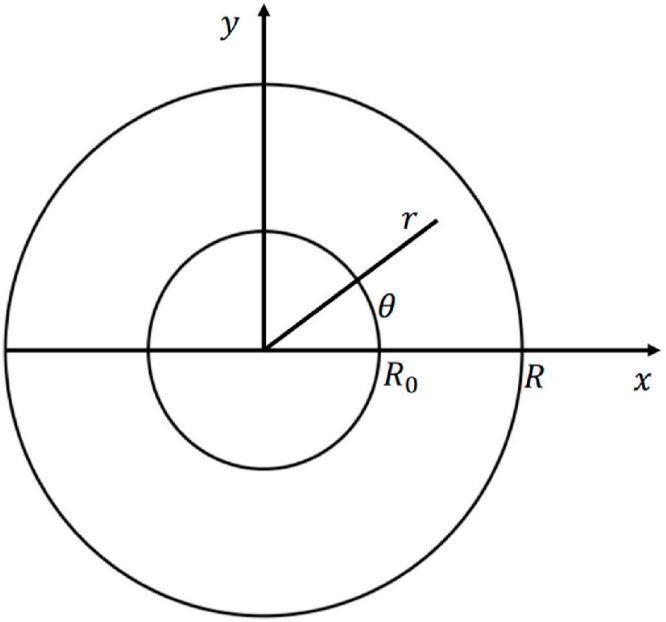

Fig. 2. Schematic diagram of a circular shelf.

$$U^{(\theta)} = \psi_r. \tag{13}$$

The governing equations can then be written

$$-r^{-1}\psi_{t\theta} - f\psi_r = -gH\eta_r + T^{(r)}, \tag{14}$$

$$\psi_{tr} - fr^{-1}\psi_\theta = -gHr^{-1}\eta_\theta + T^{(\theta)}. \tag{15}$$

Most banks are generally irregularly shaped, but the main feature is a shallow region surrounded by (much) deeper water. For a pure numerical model analysis, this poses no problems. However, for comparison with analytical results, the bank geometry must be idealized. For this reason, we adopt a bank topography which constitutes a circular version of the straight exponential continental shelf by Buchwald and Adams (1968), i.e.

$$H = \begin{cases} H_0 \exp 2b(r - R_0), & R_0 \le r \le R \\ H_0 \exp 2b(R - R_0), & r \ge R. \end{cases} \tag{16}$$

Here R_0, R define the lateral extent of the slope region; see the sketch in Fig. 3.

In our analysis, we ignore the fluid motion on top of the bank, which is assumed to be very shallow. Hence, our fluid domain is $R_0 \le r < \infty$.

In the case of exponentially increasing depth, it is advantageous to modify the stream function (Rhines, 1969; Gill, 1982) through the definition

$$\psi = H^{1/2}\,\varphi(r,\theta), \tag{17}$$

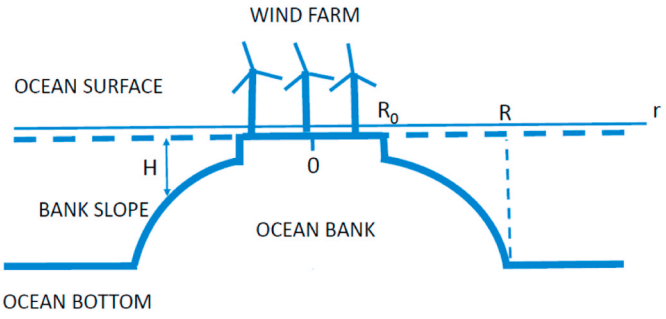

Fig. 3. Conceptual sketch of a wind farm on a shallow idealized bank.

and derive a single equation in terms of φ . Thus, by eliminating η from (14) and (15), we obtain

$$\varphi_{trr} + r^{-1}\varphi_{tr} + r^{-2}\varphi_{t\theta\theta} + \left(br^{-1} - b^2\right)\varphi_t + 2bfr^{-1}\varphi_\theta = G, \tag{18}$$

where the atmospheric forcing term G can be written

$$G = H^{-1/2}[-2bT^{(\theta)} + r^{-1}\left\{\left(rT^{(\theta)}\right)_r - T_\theta^{(r)}\right\}]. \tag{19}$$

As mentioned in Section 1, CSWs can be generated by the passage of cyclones and anti-cyclones across (or along) the shelf. In the pioneering laboratory experiments in an annular channel by Caldwell et al. (1972), this was achieved by moving a paddle periodically in the radial direction. Here, the width of the paddle was varied according to the wavelength of the expected motion. In this way, a continuous CSW frequency spectrum as function of wave number was generated. In Caldwell et al. (1972), the bottom profile was parabolic, and the correspondence between measured frequencies and numerically obtained frequencies from the governing equations, were quite good.

In the ocean, we do not expect that the wind stress will behave in such an orderly way. More likely, we will have bursts of wind of some limited duration. For an isolated structure, the spatial variation of the wind stress due to shielding will be of the same order as the structure itself. This may initiate a wave, or a group of waves, which subsequently are left to themselves.

4. Free waves on a radially symmetric shelf

The free wave motion is obtained from the homogenous part of (18). A trapped wave, after describing one complete circuit around the bank, will remain in phase with itself. Consequently, since a bottom contour is circular with circumference $L = 2\pi r$ at a given distance r from the center, a wave propagating along this contour must have a wavelength λ that satisfies $L/\lambda = m$, where m is an integer. Since the wave number k is defined by $k = 2\pi/\lambda$, we have that

$$k = m/r, \quad m = 1, 2, 3. \tag{20}$$

Hence, the wave number forms a discrete set in this case; see Longuet-Higgins (1967) for gravity waves, or Huthnance (2001) for CSWs around an island. In Fig. 4 we have sketched the wave motion around a radially symmetric shelf.

The perturbation solution for free waves in the case of radial symmetry can be written (Longuet-Higgins, 1967; Rhines, 1969) as

$$\varphi = Q(r)\exp i(kr\theta + \omega t) = Q(r)\exp i(m\theta + \omega t), \tag{21}$$

where we have used (20). Here, $Q(r)$ is the eigenfunction in the radial direction and ω is the angular wave frequency. Since the phase of CSWs in the northern hemisphere moves with shallow water to the right (Longuet-Higgins, 1965), and θ is positive in the counter-clockwise direction, the frequency ω is positive in this problem. This is demonstrated in the model calculations in Section 5. Since (21) can be written

$$\varphi = Q(r)\exp ik(r\theta + (\omega/k)t), \tag{22}$$

we realize that the phase speed c becomes

$$c = \omega/k = \omega r/m, \quad m = 1, 2, 3, . \tag{23}$$

This means that the lines of constant phase are radial, and move clockwise around the bank in time $t = L/c = m\tau$, where τ is the wave period.

By inserting (21) into (18), the equation for Q becomes:

$$Q' + r^{-1}Q' + \left[2bmf/(r\omega) + b/r - b^2 - m^2/r^2\right]Q = 0, \tag{24}$$

where the prime now denotes differentiation with respect to r. Equation (24), with given integer m and slope steepness b, defines an eigenvalue

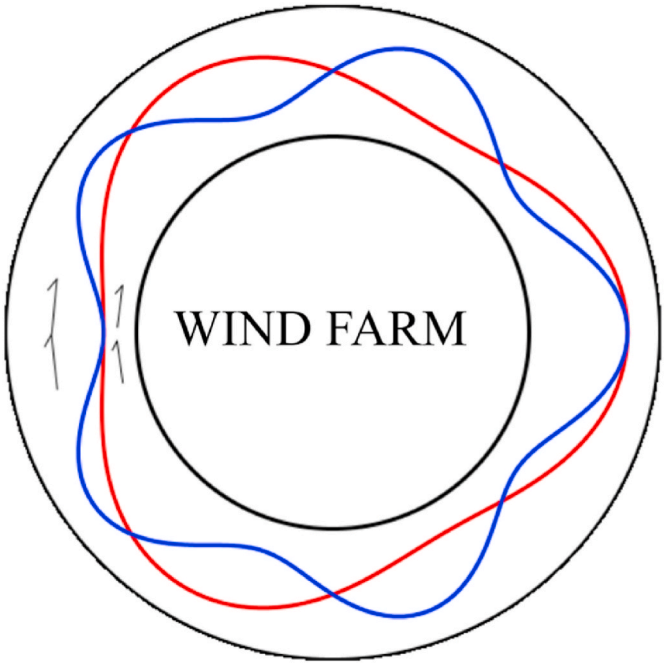

Fig. 4. Conceptual sketch of normalized radial velocities $u^{(r)}$ in CSWs around a circular shelf for $m = 3$ (red) and $m = 5$ (blue). The arrows denote direction of phase propagation (shallow water to the right in the northern hemisphere). Outer black circle corresponds to the shelf edge R in Fig. 3, and the coastal inner boundary is given by $R_0 = 0.6R$. The depicted waves propagate along the circle $r = 0.8R$.

problem for ω for known boundary values of Q at $r = R_0$, and $r = R$.

It is convenient to introduce the length scale $B = R - R_0$ into this problem. Then, we may define a non-dimensional coordinate ζ by

$$\zeta = r/B. \tag{25}$$

Now, (24) can be written

$$d^2Q/d\zeta^2 + (1/\zeta)dQ/d\zeta - [a^2 - p/\zeta + m^2/\zeta^2]Q = 0. \tag{26}$$

Here we have defined $\sigma = \omega/f$, $a = bB$ and $p = a(2m/\sigma + 1)$.

The solution of (26) for the eigenfunctions can be expressed in terms of the WhittakerM function and the WhittakerW function as

$$Q = \zeta^{-1/2}(C_1\text{WhittakerM}[p/(2a), m, 2a\zeta] + C_2\text{WhittakerW}[p/(2a), m, 2a\zeta]), \tag{27}$$

where C_1, C_2 are arbitrary constants. The WhittakerM and WhittakerW functions can be defined in terms of the hypergeometric and Kummer functions (Abramowitz and Stegun, 1965; Luke, 1969).

From the geometry in (16), we must have zero radial volume flux at $\zeta = \zeta_0 = R_0/B$. Hence,

$$Q(\zeta_0) = 0. \tag{28}$$

This means that (27) can be written

$$Q = Q_0\zeta^{-1/2}\{\text{WhittakerM}[p/(2a), m, 2a\zeta] - K_0\text{WhittakerW}[p/(2a), m, 2a\zeta]\}, \tag{29}$$

where Q_0 is a constant and

$$K_0 = \text{WhittakerM}[p/(2a), m, 2a\zeta_0]/\text{WhittakerW}[p/(2a), m, 2a\zeta_0]. \tag{30}$$

Table 1
Eigenvalues $\sigma = \omega/f$ (radial mode 1) from (37) for increasing values of m.

m	1	2	3	5	10
σ	0.094	0.178	0.231	0.312	0.335

We shall adopt the long-wave assumption in this paper. With reference to (5b), this means that we take the tangential velocity to vanish at the shelf edge $r = R$, or $\psi_r(R) = 0$. From the definition (17), this leads to

$$\varphi_r + b\varphi = 0, \quad r = R. \tag{31}$$

In (31) we have that $\varphi_r \sim (\pi/B)\varphi$. Assuming that $bB/\pi \ll 1$, the second term in (31) becomes negligibly small. Then our boundary condition at the shelf edge becomes

$$\varphi_r(r = B) = 0. \tag{32}$$

From (16), we note that this condition holds if

$$bB/\pi = (1/2\pi)\ln[H(R)/H_0] \ll 1. \tag{33}$$

We shall find that for some banks in shallow seas, suitable for wind farms, condition (33) is fairly well satisfied. It should be remembered from (20), that the discrete wavelengths for a circular shelf are given by $\lambda = 2\pi r/m$. Hence, long waves in this paper means that m must be a small integer.

In terms of Q in (21), the boundary condition at the shelf edge becomes

$$dQ/d\zeta = 0, \quad \zeta = \zeta_1 = R/B. \tag{34}$$

Applying (34), we obtain an implicit dispersion relation for the eigenfrequencies σ of this problem. Defining

$$q_1 = \zeta^{-1/2}\text{WhittakerM}[p/(2a), m, 2a\zeta], \tag{35}$$

$$q_2 = \zeta^{-1/2}\text{WhittakerW}[p/(2a), m, 2a\zeta], \tag{36}$$

the dispersion relation can be written

$$(dq_1/d\zeta)_{\zeta=\zeta_1} - K_0(dq_2/d\zeta)_{\zeta=\zeta_1} = 0, \tag{37}$$

where K_0 is given by (30).

5. Model bank

The free wave solutions are given by the geometry of the continental margin. Very shallow circular banks, or flat islands with the shelf topography described in this paper, are rarely found in nature. However, our motivation for applying the particular geometry in this paper is to reveal the physics related to shelf dynamics without having to apply numerical ocean models.

Among actual wind farm sites, the Dogger Bank in the North Sea and the Taiwan Bank in the Taiwan Strait have some features that come close to our idealized model bank. The nearly circular Taiwan bank is probably the best fit; see Liao et al. (2018). The typical topographical dimensions are: $R_0 = 60$ km, $B = 15$ km, $H_0 = 20$ m, $H(r = R) = 60$ m. In this case

$$bB/\pi = (2\pi)^{-1}\ln(H(R)/H_0) = 0.17. \tag{38}$$

Hence, (33) is fairly well satisfied. For the geometry in this example, the solutions to the dispersion relation (37) for radial mode $n = 1$ are listed in Table 1.

We note from Table 1 that $\sigma > 0$, i.e., clock-wise phase propagation with shallow water to the right, as could be anticipated from Longuet-Higgins (1965). As a check on the computed eigenvalues, we also solved the Storm-Liouville problem defined by (26), (28) and (34) by a simple numerical shooting procedure. The results confirmed those presented in Table 1.

6. Comparison between straight and radially symmetric shelves

The results in the previous section can be qualitatively understood by comparison with CSWs on a straight shelf with the coast in the x direction; see the discussion in sub-section 2.1. As in the case of a circular shelf, we consider long waves; i.e., $u(y = B) = 0$ (Buchwald and Adams, 1968; GS74). Free CSWs are governed by the homogeneous part of (4). Introducing

$$\psi = H^{1/2}\varphi(y)\exp i(kx - \omega t), \tag{39}$$

the left-hand side of (4) reduces to

$$d^2\varphi / dy^2 - \left[b^2 + k^2 - 2kfb / \omega\right]\varphi = 0. \tag{40}$$

For the long wave case, the boundary conditions are

$$\varphi = 0, \quad y = 0, \tag{41}$$

$$d\varphi/dy = 0, \quad y = B. \tag{42}$$

Hence, the solution to this eigenvalue problem can be written

$$\varphi = A \sin ly, \tag{43}$$

where

$$l = l_n = (2n - 1)\pi/(2B), \quad n = 1, 2, 3\ldots \tag{44}$$

Then, from (40), the dispersion relation becomes

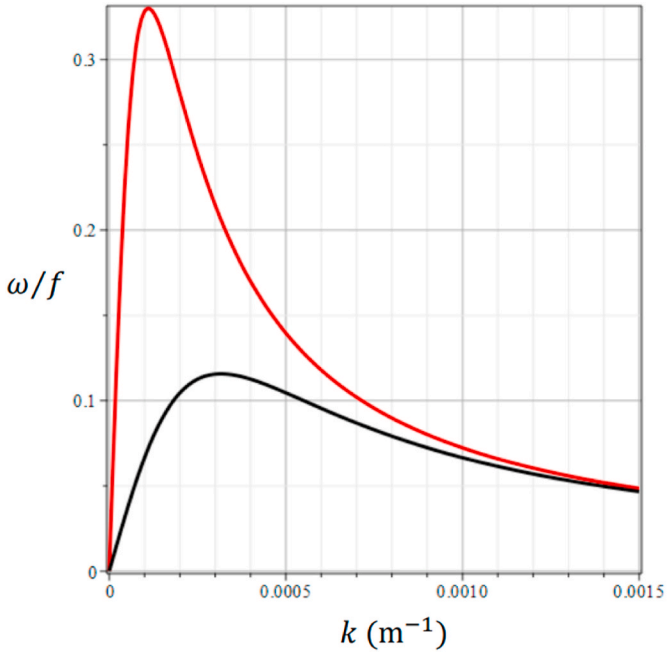

Fig. 5. Non-dimensional frequency ω/f from (45) as function of k for the first $n = 1$ (red line) and second $n = 2$ (black line) CSW mode for topographic parameters similar to an idealized Taiwan Bank; see Section 5.

$$\omega = 2kbf / \left(b^2 + k^2 + l_n^2\right). \tag{45}$$

We take that $B = 15$ km and $b = 3.66 \times 10^{-5}$ m^{-1}, as in Section 5. In Fig. 5 we have plotted ω/f as function of k for $n = 1$ and $n = 2$.

For the circular shelf discussed in Section 5, we must have $k = m/r$ to ensure that the wave remains in phase with itself after one complete circuit; see (20). To obtain a mean value for a narrow circular shelf, we assume that r corresponds to the mid line of our computational domain. Hence, the discrete set of wave numbers is given by

$$k = m/(R_0 + B/2), \quad m = 1, 2, 3, . \tag{46}$$

We now insert these discrete k values into the straight shelf dispersion relation (45). The results for mode $n = 1$ are listed in Table 2.

By comparison with the results in Table 1 for a circular shelf (values in parentheses), we note that the frequencies for discrete k-modes in a circular and a straight shelf are very similar for the geometry applied here.

A notable feature with free CSWs propagating along closed bottom contours, is that the wavelength has an upper limit and becomes discretized; see e.g., (20). From Fig. 5, we note that the admissible waves for $m \geq 1$ have $c_g = d\omega/dk > 0$. Hence, for a time-periodic wind stress with a curl in a localized area, wave energy will propagate with shallow water to the right (in the same direction as the wave phase) till the circular continental margin is filled with waves. A steady pattern is obtained when each wave remains in phase with itself after one complete circuit.

7. Forced waves on a narrow straight shelf

So far, we have studied free CSWs on a radially-symmetric shelf and compared the results with similar motion on a straight shelf. For the applied geometry, the computed eigenfrequencies become very similar. In order to investigate the response to given wind forcing, we continue with the straight shelf model. This simplifies the algebra considerably, while at the same time captures the physics involved. It should be mentioned, however, that alongshore variations in coastline curvature or offshore depth profile can create localized regions of CSW propagation with modes decaying outside these regions. This interesting problem has been discussed by Rodney and Johnson (2015), but is outside the scope of the present investigation.

For an isolated wind farm in a synoptic-scale wind field, the reduced wind stress in the down-stream wake will basically be directed normal to the isobaths. In the case of a straight shelf, this means that $T^{(x)} = 0$ in (4). Returning to our discussion of the CSW forcing in Section 1, we note that in this case, the Ekman forcing by GS74 vanishes identically. Furthermore, the normal wind stress $T^{(y)}$ will vary in the direction parallel to the isobaths over a distance D, which is of the order of the wind farm diameter.

There are basically two ways the wind field can act. Firstly, we have prevailing winds with a constant direction, varying in time. If this variation is periodical, we have a similar situation to the one modelled in the laboratory by a moving paddle across the channel. The wave generation in this case is treated in Caldwell et al. (1972), and we will not discuss it further.

Table 2
Non-dimensional frequency $\sigma = \omega/f$ and wave number from (45) and (46) for increasing values of m for the first radial mode $n = 1$. Frequencies in parentheses are values from Table 1 for a circular shelf.

m	1	2	3	5	10
k (1/m)	1.48×10^{-5}	2.96×10^{-5}	4.4×10^{-5}	7.4×10^{-5}	1.48×10^{-4}
σ	0.087 (0.094)	0.165 (0.178)	0.228 (0.231)	0.305 (0.312)	0.317 (0.335)

Secondly, the wind direction may change in time. This means that a wind-stress pulse of finite width D may move along the slope (and around the bank) at a given speed C. We will pursue this idea further. It is a novel approach, and it leads to some interesting results.

For simplicity, we take that the pulse speed C is constant. In discussing this problem for a straight shelf, we model the moving solitary pulse as

$$T^{(y)} = T - T_0 \,\mathrm{sech}[\alpha(x - Ct)], \tag{47}$$

where $\alpha = 1/D$. Here T is the constant upstream wind stress, while T_0 and α are determined by the density of wind mills and the lateral extension of the wind farm.

In this case, the only non-zero forcing term in (4) is $T_x^{(y)}$. Introducing

$$\psi = H^{1/2}\Phi(x, y, t), \tag{48}$$

we find from (4) that

$$\Phi_{txx} + \Phi_{tyy} - b^2\Phi_t - 2bf\Phi_x = H_0{}^{-1/2}T_x^{(y)}\exp(-by), \tag{49}$$

where $T^{(y)}$ is given by (47).

We solve the non-homogeneous problem (49) by expanding after the orthogonal eigenfunctions $\varphi_n(y)$ of the free wave problem (GS74). This procedure is standard, and we defer the details to Appendix A.

The general solution for the stream function (48) then becomes

$$\psi(x, y, t) = H_0 B^{-1/2}\exp(by)\sum_{n=1} F^{(n)}(x, t)\sin(l_n y). \tag{50}$$

Here l_n is defined by (44), and by replacing (x_1, t_1) by (x,t), we have from (A.14) that

$$F^{(n)}(x, t) = [a_n c_n T_0 / (2bf(c_n - C))]\left[\mathrm{sech}\,\alpha(x - Ct) - \mathrm{sech}\,\alpha(x - c_n t)\right], \tag{51}$$

where a_n is given by (A.7). We note from (50) that we get a response at two different velocities when we apply a pulse-type forcing, namely the forcing speed C, and the speed c_n of free long waves. This is similar to GS74, who considered the forcing from a wind system in the form of a long progressive wave.

8. Resonant forcing

8.1. Mathematical solution

Similar to the forcing by a long progressive wave in GS74, we notice from (51) that we have resonance when $C \to c_n$, i.e., when the forcing by the isolated pulse and the free wave travel with the same speed in the same direction. In this long-wave problem, the along-shelf wave velocity component u is much larger than the cross-shelf component. It is therefore most interesting to investigate the resonant growth of the u component. The largest values of u occurs at the boundary $y = 0$ (closest to the wind farm). From (50), with $u = -\psi_y/H$, we obtain that

$$u(y = 0) = -[T_0 / (H_0 Bbf)]\sum_{n=1}[c_n / (c_n - C)][\mathrm{sech}\,\alpha(x - Ct) - \mathrm{sech}\,\alpha(x - c_n t)], \tag{52}$$

where we have used that $b^2 \ll l_n^2$. Taking the limit $C \to c_n$, we readily find from (52) that

$$u(y = 0) = -[T_0 t / (H_0 Bbf)]\sum_{n=1} c_n \,\mathrm{sech}(\alpha(x - c_n t))\tanh(\alpha(x - c_n t)). \tag{53}$$

Thus, from (53), we find that the amplitude of u increases linearly with time in this limit. We note that resonance for long waves ($C = c_n$) is only possible if the speed of the wind-stress pulse is such that

$$C \le c_1 = 8B^2 bf/\pi^2, \tag{54}$$

where we have used that $b^2 \ll l_1^2$ in (A.10).

8.2. Numerical estimates

We note that the forced wave velocity (53) is directly proportional to the maximum sea surface wind stress deficit T_0 behind the wind farm; see (47). The determination of the deficit T_0 as function of wind speed and down-stream direction is by no means trivial. In most studies, it is not the stress deficit in the wake, but the wind speed deficit (in percent of the upstream wind) that is reported. From satellite synthetic aperture radar data for wind farms in the German Bight, Djath and Schulz-Stellenfleth (2019) report maximum deficit values ranging from 10 to 25 percent, using different estimation techniques. Christiansen et al. (2022) find that in the same region that the average maximum wind speed deficit is about 8 percent. But some of the estimates are nearly twice this value.

To assess possible hazards caused by CSWs along wind farm slopes, we should consider the generation by strong wind events lasting over several days, and also apply wind deficits above average values. As we have shown, our results for the wave kinematics of a straight shelf and a circular shelf are very similar when we apply the Taiwan Bank parameters (shelf width, depth) described in Section 5. Hence, the width of the wind stress pulse D is taken to be $2R_0$, so $\alpha = 1/D = 8.33 \times 10^{-6}\ \mathrm{m}^{-1}$ in (53). With the Taiwan bank parameters, we find that $f^2B^2/(gH_{mid}) = 0.006$, where $B = R - R_0$ and $H_{mid} = 40$ m. This means that the rigid-lid approximation discussed in Section 2 is clearly valid in this case.

The Taiwan Strait has a noticeable northeast monsoon in winter, where the wind speed on the ground could reach $24.5 - 28.4\ \mathrm{m\,s}^{-1}$ (Cheng et al., 2020). Hence, for a case study, we assume that the upstream wind velocity is $20\ \mathrm{m\,s}^{-1}$. Furthermore, from the previous discussion, we take that the maximum wind deficit is 15 percent in the wind wake. By calculating the resulting wind stresses per unit density, taking the drag coefficient c_D at the sea surface to be 1.9×10^{-3}, we find that $T_0 = 2.53 \times 10^{-4}\ \mathrm{m^2\,s^{-2}}$ in (53). In this example, we consider the gravest across-shelf mode $n = 1$. In Fig. 6, we have plotted the resonant

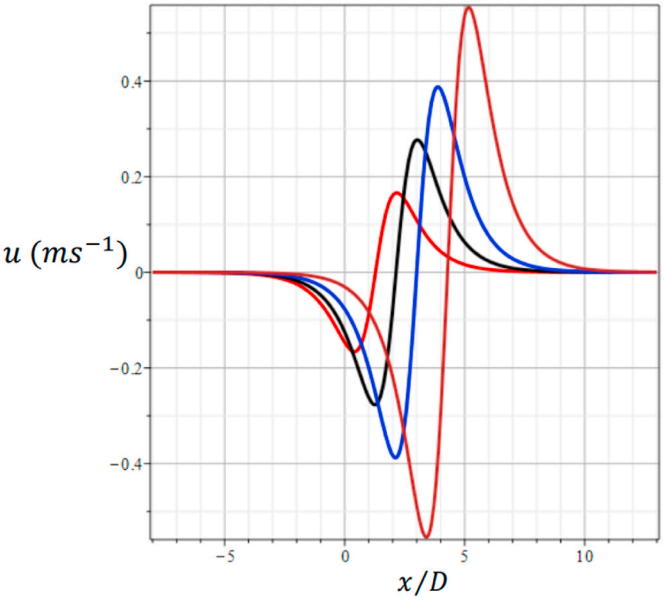

Fig. 6. Resonant horizontal along-shore wave component u at $y = 0$ as function of the non-dimensional alongshore length for $C = c_1$ at various times t. Red: $t =$ 3 days, black: $t = 5$ days, blue: $t = 7$ days, brown: $t = 10$ days.

velocity $u(y=0)$ from (53) at various times.

We note from Fig. 6 that the along-shore CSW velocity in the case of resonance is not negligible. For strong winds lasting for a week, or more, velocities at the bottom are of the order $0.4\ \mathrm{m\ s^{-1}}$. Velocities of this magnitude could potentially cause harmful erosion on the bank slopes.

For given n, all long waves move with the same phase speed (A.10). Hence the resonance on a straight shelf is not dependent of any specific wave number k, as long as it is small. This is interesting with the possible application to a circular wind farm with discrete eigenfrequencies. Then waves with small m are most likely to resonate with the forcing. It should be remarked, however, that the inclusion of a small bottom friction reduces the amplitude growth (GS74). Still, the result depicted in Fig. 6 clearly indicates that, in certain cases, a rotating external wind field forming a wind wake that travels around the bank, may induce CSWs with velocities that could cause erosion as well as affect the ecosystem on the bank slopes.

9. Discussion and concluding remarks

Electricity produced by wind farms is an adequate response to the quest for renewable energy. However, on land, such farms may come into conflict with traditional rights for animal husbandry, or the visual impact of wind farms may harm tourism. If windfarms are situated sufficiently far offshore, such problems are avoided. However, offshore windfarms may generate local problems related the marine environment; see e.g., van Berkel et al. (2020), since they often are located on shallow banks with a rich and diverse marine ecosystem.

In this paper, we consider a new aspect related to the presence of wind farms on ocean banks. We show that the wind wake due to the presence of wind turbines may induce topographic low frequency waves that propagate around the bank. Such waves may cause erosion on the bank slopes, which may damage the foundations of the wind turbines and their interconnections. This is particularly the case when resonance occurs, i.e., when the forcing field from the wind wake propagates with the same speed as that of free long waves.

As mentioned before, we are well aware that shallow banks with the topography discussed in this paper may not be found in the real ocean. The depth conditions (16) chosen here, are done for mathematical convenience. However, CSWs arising from the conservation of potential vorticity on a sloping continental margin, is a very robust phenomenon. Qualitatively, it does not depend on details of the margin, as long as it is sloping. This is clearly demonstrated in the experiments of Caldwell et al. (1972), who considered a parabolic bottom slope. We have here pointed out the possible existence of CSWs around isolated wind farms in a barotropic ocean. To the authors' knowledge, this has not been done before. Hopefully, future numerical investigations of trapped topographic waves related to offshore wind farms may benefit from the results of the present analytical study.

CRediT authorship contribution statement

Jan Erik H. Weber: Formal analysis. **Göran Broström:** Formal analysis.

Declaration of competing interest

The authors declare that they have no known competing financial interests or personal relationships that could have appeared to influence the work reported in this paper.

Appendix A. Mathematical details

In our simple case, the orthogonal eigenfunctions are; see (43):

$$\varphi_n(y) = A_n \sin(l_n y),\quad l_n = (2n-1)\pi/(2B). \tag{A.1}$$

Accordingly, we may write for the solution of (49) that

$$\Phi = \sum_{n=1} F^{(n)}(x,t)\varphi_n(y), \tag{A.2}$$

where $F^{(n)}$ is determined by the forcing term on the right-hand side. We normalize the eigenfunctions by assuming

$$\int_0^B \varphi_m \varphi_n dy = \frac{1}{2} H_0 \delta_{mn}. \tag{A.3}$$

Then,

$$A_n^2 = H_0/B. \tag{A.4}$$

Inserting (A.2) into (49), multiplying by $\varphi_m(y)$, integrate across the continental margin, and using (A.3), we arrive at

$$F^{(n)}_{txx} - \left(b^2 + l_n^2\right)F^{(n)}_t - 2bfF^{(n)}_x = a_n P(x,t), \tag{A.5}$$

where

$$P(x,t) = \alpha T_0\ \mathrm{sech}[\alpha(x-Ct)]\tanh[\alpha(x-Ct)], \tag{A.6}$$

and

$$a_n = 2l_n \,/\, \left[H_0 B^{1/2}\left(b^2 + l_n^2\right)\right]. \tag{A.7}$$

We take that the horizontal scale of the forcing field D (proportional to the diameter of the wind park) is much larger than the width of the shelf region B. This characterizes long waves on a narrow shelf. Accordingly, we may assume in (A.5) that

$$\left|F^{(n)}_{txx}\right| \ll \left(b^2 + l_n^2\right)\left|F^n_t\right|. \tag{A.8}$$

Then, we can write (A.5) as

$$c_n^{-1}F^{(n)}_t + F^{(n)}_x = -a_n P(x,t)\,/\,(2bf). \tag{A.9}$$

Here,

$$c_n = 2bf\,/\,\left(b^2 + l_n^2\right), \tag{A.10}$$

which is the speed of free long CSWs along the shelf.

The governing equation (A.9) may readily be solved by the method of characteristics; see e.g., GS74. Defining the characteristic $s = t - x/\,c_n = const.$, and $\xi = x$ as a position on the characteristic, we can take (ξ, s) as new independent variables of the problem. Hence, (A.9) can be written

$$F^{(n)}_{\xi} = -\left(a_n \alpha T_0\,/\,(2bf)\right)\mathrm{sech}[\alpha(1 - C\,/\,c_n)\xi - \alpha C s]\tanh[\alpha(1 - C\,/\,c_n)\xi - \alpha C s]. \tag{A.11}$$

We now integrate (A.11) along the characteristic $s = t_1 - x_1/c_n$ to obtain the solution at a later position (x_1, t_1). For the starting point, we assume that $x = \xi_i$, where $F^{(n)}$ vanishes. Then, by integration

$$F^{(n)}(x_1,t_1) = [a_n T_0\,/\,(2bf(1 - C\,/\,c_n))]M(x_1,t_1), \tag{A.12}$$

where

$$M = \mathrm{sech}[\alpha\{(1 - C\,/\,c_n)x_1 - C(t_1 - x_1\,/\,c_n)\}] - \mathrm{sech}[\alpha\{(1 - C\,/\,c_n)\xi_i - C(t_1 - x_1\,/\,c_n)\}] \tag{A.13}$$

Initially, we assume that the wind stress starts acting at $t = 0$ when $x = \xi_i$. Then, since $x - c_n t = x_1 - c_n t_1$, we have that $\xi_i = x_1 - c_n t_1$. Inserting into (A.13), we find

$$F^{(n)}(x_1,t_1) = [a_n c_n T_0\,/\,(2bf(c_n - C))]\left[\mathrm{sech}\,\alpha(x_1 - Ct_1) - \mathrm{sech}\,\alpha(x_1 - c_n t_1)\right]. \tag{A.14}$$

References

Abramowitz, M., Stegun, I., 1965. Handbook of Mathematical Functions. Dover Publications.

Brink, K.H., 1983. Low frequency free wave and wind-driven motions over a sub-marine bank. J. Phys. Oceanogr. 13, 103–116.

Brink, K.H., 1991. Coastal-trapped waves and wind-driven currents over the continental shelf. Annu. Rev. Fluid Mech. 23, 389–412.

Broström, G., 2008. On the influence of large wind farms on the upper ocean circulation. J. Mar. Syst. 74, 585–591.

Buchwald, V.T., Adams, J.K., 1968. The propagation of continental shelf waves. Proc. Roy. Soc. Lond. 305, 235–250.

Caldwell, D.R., Cutchin, D.L., Longuet-Higgins, M.S., 1972. Some model experiments on continental shelf waves. J. Mar. Res. 30, 39–55.

Cheng, K.-S., Ho, C.-Y., Teng, J.-H., 2020. Wind characteristics in the Taiwan Strait: a case study of the first offshore wind farm in Taiwan. Energies 2020 13, 6492. https://doi.org/10.3390/en13246492.

Christiansen, N., Daewel, U., Djath, B., Schrum, C., 2022. Emergence of large-scale hydrodynamic structures due to atmospheric offshore wind farm wakes. Front. Mar. Sci. 9, 1–17.

Djath, B., Schulz-Stellenfleth, J., 2019. Wind speed deficits downstream offshore wind parks - a new automised estimation technique based on satellite synthetic aperture radar data. Met. Zeitsch. (Contrib. Atmos. Scien.) 28 (6), 499–515.

Gill, A.E., 1982. Atmosphere-Ocean dynamics. Int. Geophys. Ser., vol 30 Academic Press, p. 662.

Gill, A.E., Schumann, E.H., 1974. The generation of long shelf waves by the wind (GS74). J. Phys. Oceanogr. 4, 83–90.

Huthnance, J.M., 2001. Coastal trapped waves. Encyclopedia of Ocean Sciences 87–94.

Liao, E., Oey, L.Y., Yan, X.-H., Li, L., Jiang, Y., 2018. The deflection of the China coastal current over the Taiwan Bank in winter. J. Phys. Oceanogr. 18, 1433–1450.

Longuet-Higgins, M.S., 1965. Some dynamical aspects of ocean currents. Quart. J. R. Met. Soc. 91, 425–451.

Longuet-Higgins, M.S., 1967. On the trapping of wave energy round islands. J. Fluid Mech. 29, 781–821.

Luke, Y., 1969. The Special Functions and Their Approximations, vol 1. Academic Press, 1969.

Rhines, P.B., 1969. Slow oscillations in an ocean of varying depth Part 2. Islands and seamounts. J. Fluid Mech. 37, 191–205.

Rodney, J.T., Johnson, E.R., 2015. Localized continental shelf waves: geometric effects and resonant forcing. J. Fluid Mech. 785, 54–77.

van Berkel, J., Burchard, H., Christensen, A., Mortensen, L.O., Petersen, O.S., Thomsen, F., 2020. The effects of offshore wind farms on hydrodynamics and implications for. Fish. Oceanogr. 33, 108–117.

Weber, J.E., Drivdal, M., 2012. Radiation stress and mean drift in continental shelf waves. Continent. Shelf Res. 35, 108–116.

Further reading

Buchwald, V.T., Kachoyan, B.J., 1987. Shelf waves generated by coastal flux. Aust. J. Mar. Freshw. Res. 38, 429–437.